Local Atomic Environment of the Cu-related Defect in Zinc Oxide

To cite this article before publication: Gray et al, 2017, J. Phys. D: Appl. Phys., at press:
https://doi.org/10.1088/1361-6463/aa5f07

Local Atomic Environment of the Cu-related Defect in Zinc Oxide

Ciarán Gray[1,*], Lukas Trefflich[2,∀], Robert Röder[2], Carsten Ronning[2], Martin O. Henry[1], Enda McGlynn[1,*]

[1] *School of Physical Sciences, National Centre for Plasma Science and Technology, Dublin City University, Glasnevin, Dublin 9, Ireland.*

[2] *Institute of Solid State Physics, Friedrich-Schiller-University of Jena, 07743 Jena, Germany.*

*Authors to whom correspondence should be addressed: ciaran.gray5@mail.dcu.ie, enda.mcglynn@dcu.ie.

ABSTRACT

Zn- and O- isotopically enriched ZnO nanorods were grown with excellent optical quality allowing an identification and resolution of various bound exciton zero phonon lines. Furthermore, the well-known Cu-related emission at 2.86 eV could specifically be studied in order to investigate the local environment of the defect including possible involvement of native defects such as interstitials and vacancies in this deep centre. Energetic shifts of this zero phonon line were measured and compared to changes in the near band edge energies as a function of the enrichment. No relative shift was observed in Zn-enriched samples, indicating that only O atoms lie in the immediate vicinity of the Cu atom, and that Zn interstitials and O

[∀] *Now at the Institute for Experimental Physics II, University of Leipzig, 04103 Leipzig, Germany.*

vacancies are not involved in this defect. Near band edge and Cu 2.86 eV ZPL emissions in samples with O-enrichment displayed a significant relative shift and the Cu 2.86 eV ZPL line widths showed a substantial increase, which is attributed to the multiple local configurations possible for O atoms surrounding the Cu atom in these mixed isotope environments. These data provides the first direct evidence of the microscopic nature of this defect centre of a Cu atom substituting on a Zn lattice site and is thus consistent with the conventional model of this defect.

1. INTRODUCTION

An area of particular interest in the literature has been the production of ZnO nanorods for use in optical and optoelectronic applications including photodetectors (photodiodes and photovoltaics)[1,2], UV emitters such as LEDs[3] and laser diodes [4–8] transparent conducting oxides (TCO) in solar cells and as a transistor material.[9–11] These materials have been produced using a number of growth methods including chemical bath deposition (CBD), vapour phase transport (VPT), chemical vapour deposition (CVD) and hydrothermal deposition.[10,12–17] The optical properties of these materials are mainly determined by the nature and concentration of defects and impurities in the materials.[18] Thus, characterisation and understanding of such defect species is crucial for the ultimate application of the ZnO nanorods. Furthermore, isotopic enrichment is an established technique in the study of crystal structure and impurities in semiconductor materials such as ZnO.[19–24] There has been a reasonable amount of studies of free exciton (FX) photoluminescence (PL) and Raman behaviour in isotopically enriched ZnO, but much fewer studies on bound exciton (BX) emissions.[25–30]

The application of ZnO material in optoelectronic devices may be affected by both deeper level defects near the middle of the band gap as well as the shallow defects causing bound exciton emission such as the I-lines in PL. The Cu-related emission at 2.86 eV in ZnO is one such deep radiative defect centre yielding a bright, structured, wide emission band peaking in the green visible region, referred to as the structured green band (SGB). It comprises a zero phonon line (ZPL) at 2.86 eV and a series of longitudinal optical (LO) replicas separated by ~72 meV showing strong electron-phonon coupling.[31] Although the emission spectrum of ZnO had been studied for some time, the origin of this SGB was not certain when R. Dingle made one of the most fundamental contributions to the discussion in 1969.[32] He presented strong, albeit not definitive, evidence that this SGB resulted from a transition involving a single Cu impurity on a Zn site (Cu_{Zn}) in a Cu^{2+} charge state acting as a neutral deep acceptor. [32,33] Despite Dingle's work, and extensive studies concerning the green band,[34–36] some disagreement persisted regarding its nature,[4,37] and it was not until much more recently that Cu involvement was unambiguously confirmed as the cause of the SGB emission by Byrne *et al*.[33] These data, in addition to Dingle's data on the *g*-factor and stress measurements, were consistent with the assignment of this defect as a single substitutional Cu^{2+} atom on a Zn site. Byrne *et al*.[33] also discussed in some detail the possible role of the different valence states of Cu on the SGB as well as the relationship of the SGB to the unstructured green band, normally attributed to oxygen vacancies. However, the studies left open whether a complex of Cu_{Zn} with other defects along the *c*-axis, for example Cu_{Zn}-V_O or Cu_{Zn}-V_{Zn} complexes, could be present and therefore the exact defect structure, in terms of the local environment of the Cu atom was not fully determined. Isotopically enriched ZnO nanorods of excellent quality present an opportunity for a detailed study of the Cu-related emission at 2.86 eV and its associated phonon sideband for revealing the local environment of the defect.

We have recently reported the growth of isotopically enriched ZnO nanorods grown using three novel methods.[38,39] Here, we report a combined optical study of both Zn- and O-isotopically enriched ZnO nanorods whose very high structural and optical quality allows detailed study of their optical properties at low temperatures concerning shallow and deep defect emission centres. Specifically, the near band edge (NBE) and the Cu-related SGB 2.86 eV ZPL data for such enriched ZnO materials are investigated and the effects of enrichment on the Cu-related defect at 2.86 eV is examined to further determine the local environment of the defect responsible. These data and analyses provide the first direct evidence in support of the model proposed in Dingle's original work of this defect being composed of a single substitutional Cu atom on a Zn site with nearest neighbour O atoms.

2. MATERIALS AND METHODS

The detailed growth methods employed are described in references [38,39]. In short, the Zn-isotopically enriched samples were grown using a three-step process involving a drop-coated seed layer, and buffer layer of ZnO nanorods grown by chemical bath deposition (CBD) and finally isotopically enriched ZnO nanorods grown by carbothermal reduction vapour phase transport (CTR-VPT) using Zn-enriched source powders.[38] CBD and VPT are common methods used to grow ZnO nanorods.[10,12,13,15,40] The growth method used here was developed in our group and was based upon other work both in our group and reports in the literature.[13,14,41] The Zn-enriched samples in table 1 were grown using this method. The actual Zn enrichments were very close to the nominal values, confirmed by SIMS data.

Oxygen-isotopically enriched ZnO nanorods were grown by two methods as previously reported.[39] The CTR-VPT growth process is based on the reduction of ZnO powder by the graphite to produce Zn vapour and carbon monoxide (CO). The Zn vapour is then re-oxidised in a vapour-solid (VS) process at the energetically favourable sites provided by the aligned CBD buffer layer using residual O_2 present in the tube during growth (rather than the O initially in the ZnO powder, which is captured by C to form CO). In order to grow ZnO nanorods enriched with ^{18}O isotopes, the residual O_2 was removed from the tube, and then $^{18}O_2$ gas introduced. Three samples were produced using this method: natural $Zn^{16}O$ by evacuating the tube and re-filling with $^{16}O_2$ and N_2, isotopically enriched ZnO by re-filling with $^{18}O_2$ and N_2, and a mixed 50:50 $Zn^{16/18}O$ sample by using a mixture of both oxygen isotopes with N_2. They are labelled as the 'VS' samples, grown using method 1. The actual ^{18}O enrichments, albeit substantial, differ from the nominal values by a considerable amount due to a variety of unanticipated sources of ^{16}O contamination and the actual enrichments are given in table 2 below. Details are given in reference [39].

The second method used to grow O-enriched ZnO nanorods made use of direct oxidation of Zn metal to "trap" the ^{18}O to form a $Zn^{18}O$ powder, which could then be used in a vapour-liquid-solid (VLS) VPT growth method. In this case, the ZnO source powder provides both the Zn and O_2 vapours for subsequent growth due to the sublimation of the ZnO powder. The enriched ZnO source powder was produced by oxidising Zn metal powder with enriched $^{18}O_2$ gas. ZnO nanorods were then grown using this source powder in a VLS process using Au as a catalyst, based on previous work.[42,43] The Au coating melts and forms droplets on the substrate, which act as energetically favourable nucleation sites. The furnace then cooled overnight before the samples were removed. Three samples were produced with this method: $Zn^{16}O$, $Zn^{18}O$ and mixed 50:50 $Zn^{16/18}O$. They are labelled 'VLS' grown using method 2. Table 2 summarises the O-enriched samples. Note, the actual

^{18}O enrichments, albeit substantial, differ from the nominal values by a considerable amount due to a variety of unanticipated sources of ^{16}O contamination. The ^{18}O enrichments were estimated at 60% for Zn^{18}O-VS, 35% for Zn^{18}O-VLS, 40% for Zn$^{16/18}$O-VS and 25% for Zn$^{16/18}$O-VLS, with an error of ±5% in all cases as given in table 2 below.[39] Typical morphologies observed in isotopically enriched nanorods are displayed in figure 1 for one Zn enrichment (^{64}Zn) and one O enrichment (^{16}O/^{18}O) level and further data is shown in references [38,39].

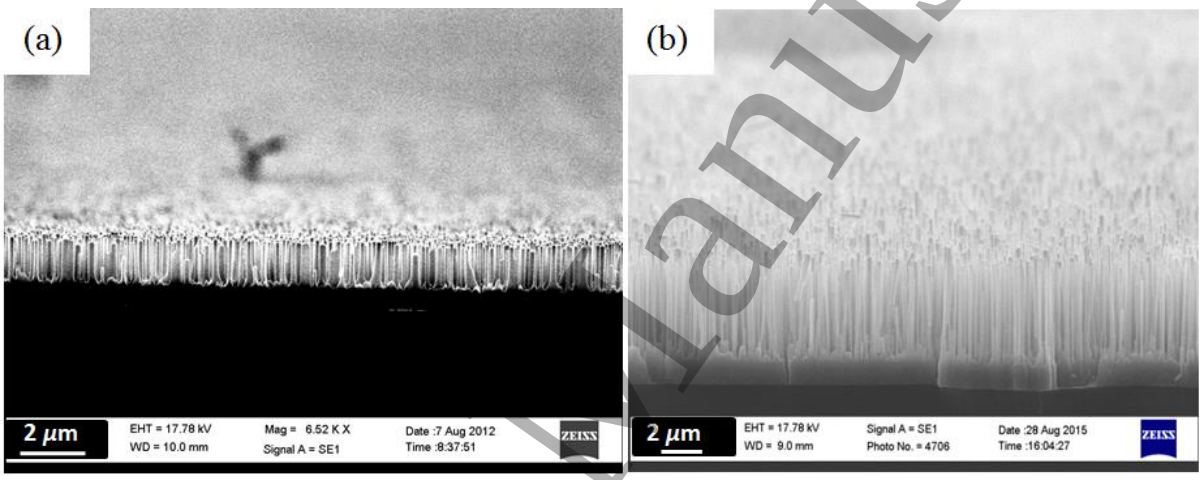

Figure 1: Typical morphologies of isotopically enriched ZnO: (a) ^{64}ZnO and (b) Zn$^{16/18}$O.

Table 1: Zn isotopically enriched ZnO nanorods samples, grown by vapour transport techniques, as a function of the degree of enrichment.

Label	Description
^{64}ZnO	^{64}Zn
^{66}ZnO	^{66}Zn
^{68}ZnO	^{68}Zn
^{nat}ZnO	Natural Zn isotopic distribution, avg. = $^{65.4}$Zn

Table 2: Oxygen isotopically enriched ZnO nanorods samples, which were grown by vapour transport techniques, as a function of the degree of enrichment.

Label	Nominal Enrichment	Measured Enrichment[39]	Description
$Zn^{16}O$-VS	$Zn^{16}O$	-	Method 1: O enriched ZnO nanorods grown by the VS method
$Zn^{16/18}O$-VS	$Zn^{16/18}O$	40% ^{18}O	
$Zn^{18}O$-VS	$Zn^{18}O$	60% ^{18}O	
$Zn^{16}O$-VLS	$Zn^{16}O$	-	Method 2: O enriched ZnO nanorods grown by the VLS method
$Zn^{16/18}O$-VLS	$Zn^{16/18}O$	25% ^{18}O	
$Zn^{18}O$-VLS	$Zn^{18}O$	35% ^{18}O	

All of the samples are of excellent structural quality with preferential nanorod growth along the *c*-axis as shown by SEM and XRD in previous reports.[38,39] PL was carried out using a 325 nm HeCd laser as the excitation source directed onto the sample in a Janis model SHI-950-5 cryostat at ~14 K and a diffraction grating spectrometer system. The spectroscopic system consisted of a 1 m model SPEX 1701 monochromator and Hamamatsu model R3310-02 photomultiplier tube, which was cooled to approximately -20 °C. The monochromator contained a grating blazed at 330 nm (ISA model 510-05). A Hg spectral lamp was placed on the optical table such that some of its emission also scattered into the spectrometer entrance slit. The spectral lines from this lamp were used to calibrate the spectra recorded to correct for minor irreproducibility from scan to scan. In addition, the spectra have been corrected for the refractive index of air. Each sample was also examined using an additional system, a Bomem DA8 FT spectrometer and IPH8200L PMT detector with a second cryostat, a Janis Research CSS-550 cooled to ~19 K. Note that the results from both systems were in perfect agreement. A portion of some samples was annealed for ten

minutes at 900˚C in the same oxygen isotopic environment as used during their growth to increase the green band intensity for some measurements.[44,45]

3. RESULTS AND DISCUSSION

3.1. Zn-enriched Nanorods

Figure 2 shows the NBE and Cu-related 2.86 eV ZPLs for the Zn-enriched samples. . The dominant feature in the near band edge region is the I_9 line attributed to In impurities, which is of particular interest for the purposes of our subsequent analysis, as described below.[46] The I_8 and I_6 lines attributed to Ga and Al impurities are also clearly observed.[46–48] The I_2 line attributed to ionised In impurities[49] and the surface exciton[50] (SX) emission are also visible and labelled in figure 2(a). These common impurities most probably come from the laboratory environment where the growth takes place, for example from the alumina boat, or the source powders. Representative deep level Cu-related 2.86 eV SGB ZPL spectra are shown in figure 2(b).

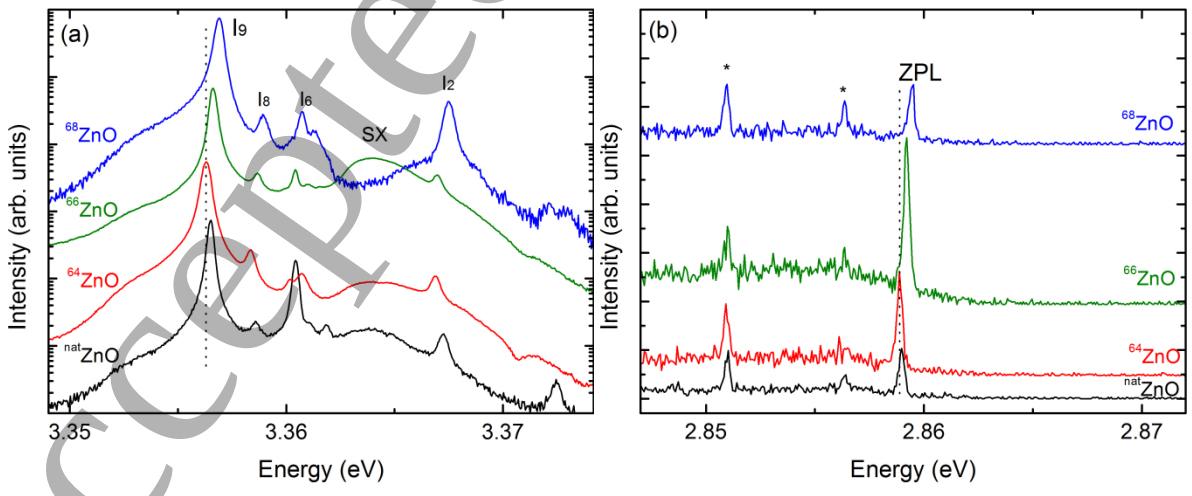

*Figure 2: NBE (a) and Cu-related 2.86 eV ZPL (b) high-resolution spectra from the Zn-enriched samples (spectra shifted vertically for clarity). The dashed vertical line is at the ^{64}Zn I_9/ZPL energy. The smaller peaks at lower energies than the ZPL are caused by the Hg calibration lamp, as marked with *, and thus do not shift in energy.*

3.2. O-enriched Nanorods

Figure 3 displays typical NBE and Cu-related 2.86 eV ZPL spectra for the O-enriched nanorods. Specifically, figures 3(a) and 3(c) show the NBE regions in the VS and VLS samples. The NBE region is dominated by the I_9 and I_6 lines.[48,51] Further NBE lines also appear in some samples. Figure 3(b) shows the Cu-related 2.86 eV ZPL line in the VS samples and figure 3(d) shows those in the VLS samples. These are typical of the Cu-related 2.86 eV ZPL lines seen in all the O-enriched samples. Note that the other lines in the ZPL spectra in this region are again from the Hg calibration lamp. The VS samples were all annealed to activate the SGB, while the VLS samples required no such an annealing as the SGB was present in as grown materials. Similar to the Zn-enriched samples, these BX and Cu impurities are common in ZnO and most probably are due to the growth environment, i.e. source powders and the boats and tubes used.

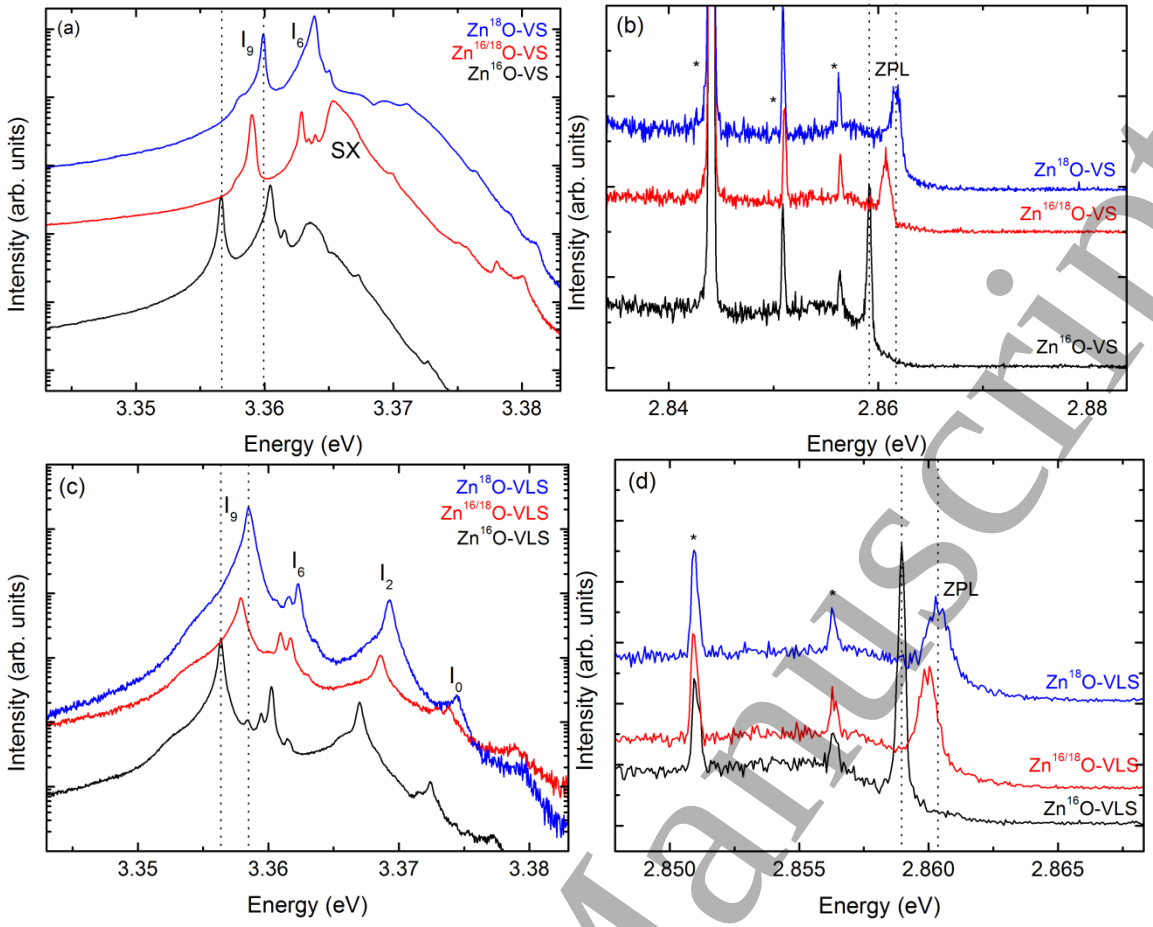

*Figure 3: NBE (a, c) and Cu-related 2.86 eV ZPL (b, d) spectra from the VS and VLS O-enriched samples (spectra shifted vertically for clarity). The vertical lines mark the I_9 ZPL of the $Zn^{16}O$ and $Zn^{18}O$ nanorods. The smaller peaks at lower energies than the ZPL are due to the Hg calibration lamp, marked with *, and thus do not shift in energy.*

The shifts to higher energies with increasing O isotopic mass, for both the BX-lines and Cu-related 2.86 eV ZPL regions, are readily apparent in figure 3. We note that the BX-line widths (< 1 meV) are far narrower than the < 5 meV and 2-8 meV for O-enriched ZnO reported by previous authors.[52,53] Furthermore, a clear increase in the line width of the Cu-related 2.86 eV ZPL lines occurs from the $Zn^{16}O$ samples to the $Zn^{18}O$ samples, which is not seen for the BX-lines. We note also that the Cu-related 2.86 eV ZPL for the O-enriched

samples, presented in figure 3(b) and (d), clearly shows a broadening moving from $Zn^{16}O$ to $Zn^{18}O$, which is not seen for the NBE BX-lines.

3.3 Energy shifts and line widths for Zn-enriched Nanorods

In order to investigate the effects of the Zn isotopic changes on the local defect environment on the Cu-related 2.86 eV ZPL and associated SGB in ZnO, we compare the shifts and line widths in exciton recombination energies in the NBE region with those of the Cu-related 2.86 eV ZPL. NBE emission energy shifts were observed in these samples when the isotopic content of the crystal was changed,[38,39] due to the change in mass and corresponding change in the energy of the crystal vibronic states due to the isotope effect. However, we expect that the local defect environment (essentially the nearest neighbour ligand species) of the defect responsible for the Cu-related 2.86 eV ZPL should be a dominant contributor to the vibronic energy of the deep defect, and thus, if the Cu atom occupies an O site or if there are local Zn interstitials (Zn_i) or O vacancies (V_O) in the defect complex, we should observe a different shift for the Cu-related ZPL compared to the NBE BX emissions, which are characteristic of the crystal as a whole, in the Zn enriched samples.

The position of the In-related I_9 BX recombination was selected as a reference energy to measure changes in the NBE emission positions with changing isotope enrichment. The line widths of the I_9 lines in these samples were in the range 0.31-0.44 meV with no particular trend evident regarding changes with isotopic mass. The line widths of the Cu-related 2.86 eV ZPL lines were ~0.3 meV.

For the Zn-enriched samples, the positions of the I_9 lines and Cu-related 2.86 eV ZPL lines are shown in figure 4. The left hand y-axis (black) shows the I_9 energies, and the right hand y-axis (blue) shows the Cu-related 2.86 eV ZPL energies. The I_9 axis covers the range 3.3559 - 3.357 eV, and the Cu-related 2.86 eV ZPL energy axes also covers an energetic range of 1.1 meV but with this axis shifted to align the Cu-related 2.86 eV ZPL energy and the I_9 energy in the ^{64}ZnO sample at the same point on each graph. Thus, the relative shifts of both the I_9 and Cu-related 2.86 eV ZPL energies in each sample with changing isotopic composition can be compared.

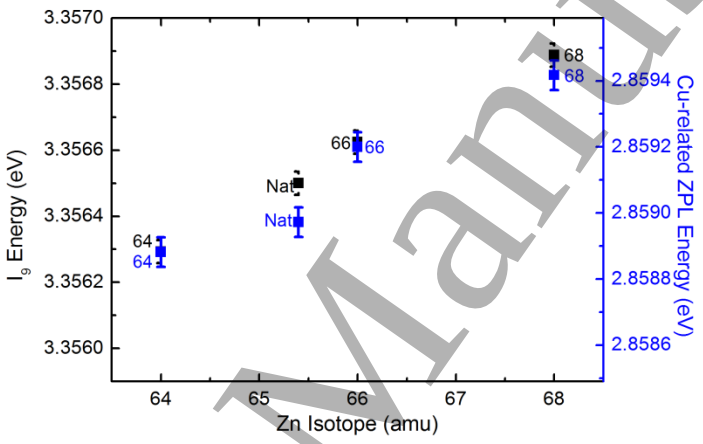

Figure 4: Energies of the I_9 lines (black squares) and Cu-related 2.86 eV ZPL lines (blue squares) in the Zn-enriched ZnO samples. The error bars represent the resolution for each scan to give an indication of the accuracy of the positions: ±0.035 meV for the I_9 lines and ±0.045 meV for the Cu-related 2.86 eV ZPL.

The I_9 energy increases with increasing Zn isotopic mass from ^{64}ZnO to ^{68}ZnO by 0.6 meV. Similarly, the Cu-related 2.86 eV ZPL energy increases by 0.54 meV. The trends shown in figure 4 clearly indicate that there is a consistent increase in I_9 and Cu-related 2.86 eV ZPL line positions from ^{64}ZnO to ^{68}ZnO of ~ 0.6 meV. The relative energy shifts between

the two emissions are therefore as small as ~0.1 meV, within the experimental error considering the scan resolutions.

The shifts in the I_9 and Cu-related 2.86 eV ZPL positions are of the same order as those reported previously for ZnO single crystals.[52,53] There appears to be neither a significant excess shift in Cu-related 2.86 eV ZPL position relative to the NBE position nor any change in line width of this feature. Furthermore, there is no significant change in line width of the I_9 line in the samples. Hence, the absence of a discernible relative spectral shift, in addition to the constant line width of the I_9 and Cu-related 2.86 eV ZPL features for all Zn-enriched samples shows clearly that the Cu impurity in not in a Zn-dominated environment. Thus supports the assignments from previous work that the Cu atom in this defect is on a Zn site and therefore surrounded by O.[32,33] This result also provides very strong evidence that there is no involvement of either Zn_i or V_O native defect complexing in the Cu-related 2.86 eV ZPL and SGB emission in ZnO. The involvement of either the Zn_i or V_O native defects would mean that the local defect environment would have a dominant contribution to the vibronic energy of the deep defect determined by the Zn mass, which would lead to a different shift for the Cu-related ZPL compared to the NBE BX emissions, contrary to our observations.

3.4 Energy shifts and line widths for O-enriched Nanorods

Figure 5 shows the energies of the I_9 and Cu-related 2.86 eV ZPL lines in each VS and VLS O-enriched sample. In each graph, the left hand y-axis (black) shows the I_9 energies, and the

right hand y-axis (blue) shows the Cu-related 2.86 eV ZPL energies. The axes are aligned in a similar way to figure 4.

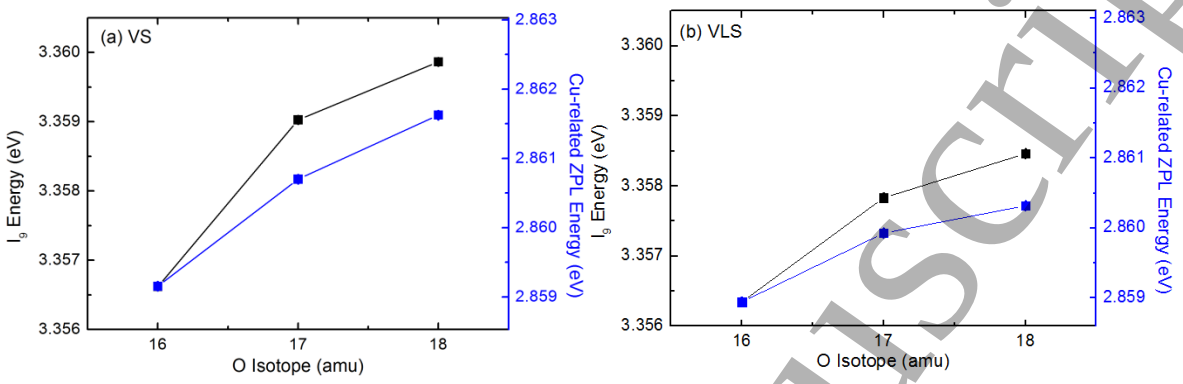

Figure 5: Energies of the I_9 lines (black) and Cu-related 2.86 eV ZPL lines (blue) in the (a) VS, and (b) VLS O-enriched ZnO samples. The error bars represent the resolution for each scan to give an indication of the accuracy of the positions: ±0.035 meV for the I_9 lines and ±0.045 meV for the Cu-related 2.86 eV ZPL.

The increases in the energies of both the I_9 and Cu-related 2.86 eV ZPL lines are clearly shown in figure 5. This indicates that isotopic enrichment with different compositions of O isotopes has been successful. However, there are a number of points to note while examining these energy shifts as described below. Table 3 summarises the shifts observed between the $Zn^{16}O$ and $Zn^{18}O$ samples, and between the $Zn^{16}O$ and $Zn^{16/18}O$ samples, for the I_9 and Cu-related 2.86 eV ZPL lines, in both the VS and VLS samples. The ratio of the I_9 shifts to the Cu-related 2.86 eV ZPL shifts in each case is also shown in the table. The lines shift monotonically with isotopic enrichment, but the ratio the ratio of the I^9 energy shift to 2.86 eV ZPL shift remains roughly constant in our data.

Table 3: Summary of the NBE and Cu-related 2.86 eV ZPL energy shifts in the O-enriched samples.

	I_9 energy shift from $Zn^{16}O$ to $Zn^{18}O$ (meV)	**Cu-related 2.86 eV ZPL energy shift from $Zn^{16}O$ to $Zn^{18}O$ (meV)**	**Ratio of I_9 and Cu-related ZPL shifts ($Zn^{16}O$ to $Zn^{18}O$)**	**I9 energy shift from $Zn^{16}O$ to $Zn^{16/18}O$ (meV)**	**Cu-related 2.86 eV ZPL energy shift from $Zn^{16}O$ to $Zn^{16/18}O$ (meV)**	**Ratio of I_9 and Cu-related ZPL shifts ($Zn^{16}O$ to $Zn^{16/18}O$)**
VS samples	3.24	2.47	1.31	2.41	1.55	1.55
VLS samples	2.11	1.37	1.54	1.48	0.98	1.51

As reported previously[39], the I_9 energy shifts between the $Zn^{16}O$ and $Zn^{18}O$ samples are less than those reported in the literature for the same nominal degree of ^{18}O enrichment. This shows that our samples are not fully isotopically enriched as would be expected from the nominal enrichments associated with the growth processes. The phonon energies measured by Raman spectroscopy for these samples previously reported also support this observation.[39] The reasons for this have been reported in more detail elsewhere and are most likely due to sources of oxygen already chemically bound within the growth system which can move into the growing nanorods, by some process of exchange with the ^{18}O, with some additional contribution of ^{16}O from ZnO residue on the tube and boat in the case of the VLS samples due to the higher temperatures used in that method.[39]

Regarding the present study, it is clear from table 3 that the shifts in the Cu-related 2.86 eV ZPL energies in all the O-enriched samples are less than the corresponding shifts in the NBE region. This is observed across the VS and VLS samples. For example, the I_9 shift

in the VS samples is 3.24 meV, but the Cu-related 2.86 eV ZPL shift is just 2.47 meV. Likewise, the I_9 shift in the VLS samples is 2.11 meV, but the Cu-related 2.86 eV ZPL shift is just 1.37 meV, respectively. These differences are much larger than the error bars associated with the values. The key factor is that the ratio of the shifts is quite different from 1 in all cases. These data clearly show that the oxygen mass has a dominant effect on the Cu-related 2.86 eV ZPL, indicating that the local environment of the Cu atom interacts strongly with O species. This interaction occurs with either O atoms on (or close to) lattice sites around the Cu atom on the Zn site and/or due to the presence of O_i or V_{Zn} native defects complexing with the Cu atom on the Zn site (since the contribution of a V_{Zn} defect will be determined by the oxygens surrounding the vacancy).

The FWHM of the Cu-related ZPL increases from 0.44 meV to 1.18 meV between Zn16O and Zn18O in the VS samples, and from 0.36 meV to 0.93 meV for the VLS samples. Given the deep nature of the defect with tightly bound carriers, the broadening observed for the Cu-related 2.86 eV ZPL is explained by the imperfect isotopic enhancement, because there exist a number of different configurations for the four O atoms surrounding the Cu. Thus, there are varying possible combinations of ^{16}O and ^{18}O atoms that the Cu atom could be adjacent to such as 4 x ^{16}O, 1 x ^{18}O + 3 x ^{16}O etc. The NBE DX emissions should not be broadened to the same degree since their larger excitonic Bohr radius leads to an averaging over a number of unit cells.[54] However, some broadening occurs at least in the intentionally varied $Zn^{16/18}O$ sample, which is consistent with the observations for the Cu SGB emission.

Ultimately, because of the small line shifts and the inability to resolve lines associated with individual O atomic configurations, we do not have enough information to determine whether the origin of the effects we see upon O isotopic enrichment is due to O atoms on (or

close to) lattice sites around the Cu atom or the presence of O_i or V_{Zn} native defects complexing with the Cu atom at the defect. However, we consider it far more likely that the origin is the former effect (i.e. Cu substituting on a Zn lattice site surrounded by O atoms), as this would agree with the previous work of Dingle[32] and Byrne *et al.*[33], in terms of the defect symmetry (C_{3v})[55] and other known aspects of the defect. The likelihood of a complex of a Cu atom with three native defects (O_i or V_{Zn}) producing a defect with overall C_{3v} symmetry is very small. The starting configuration of the 4 O atoms surrounding the Zn site on which the Cu atom substitutes has this symmetry naturally, and it seems a far more likely explanation that any relaxation of the surrounding O after Cu substitution will maintain this symmetry. Thus our data overall support the model of Dingle[32] of a single Cu atom on a Zn site surrounded by O atoms on (or close to) lattice sites.

CONCLUSIONS

This low temperature PL study of Zn-enriched and O-enriched ZnO nanorods has shown that the optical quality of all samples was excellent, and that all samples displayed intense NBE emissions with narrow linewidths, which are in many cases far narrower than those reported previously in the literature. The Cu-related SGB was also present in all samples, although some samples required annealing to increase its intensity to allow detailed spectroscopic study. The Zn-enriched samples displayed a shift of ~0.6 meV as the isotopic composition changes from ^{64}ZnO to ^{68}ZnO for both the I_9 BX recombination and the Cu-related 2.86 eV ZPL and no changes in line width of either emission with changes in isotopic composition. This indicates that Zn atoms do not contribute to the local defect environment in the Cu-related defect at 2.86 eV. The O-enriched samples displayed a NBE emission shift

of 3.24 meV as the isotopic content changed from $Zn^{16}O$ to $Zn^{18}O$ for the VS samples, and a smaller shift of around 2.11 meV for the VLS samples. Relative shifts and larger line width broadening for the Cu-related 2.86 eV ZPL versus the NBE in the O-enriched samples can be attributed to the contribution of O to the local defect environment adjacent to the Cu on a Zn site, most likely due to the O atoms on (or close to) lattice sites surrounding the Cu atom substituting on the Zn lattice site. This conclusion is fully in agreement with the previous work of Dingle[32] and Byrne *et al.*[33] and is the first direct evidence in support of this model for the defect.

ACKNOWLEDGEMENTS

CG and EMcG gratefully acknowledge the Irish Research Council (IRC) for a postgraduate scholarship under the EMBARK initiative. This work financially supported by the Deutsche Forschungsgemeinschaft (DFG) within the frame of the research unit FOR1616.

REFERENCES

[1] Teng F, Zheng L, Hu K, Chen H, Li Y, Zhang Z and Fang X 2016 A surface oxide thin layer of copper nanowires enhanced the UV selective response of a ZnO film photodetector *J. Mater. Chem. C* **4** 8416–21

[2] Kakazey M, Vlasova M, Juarez-Arellano E A, Torchynska T and Basiuk V A 2016 Defect states and morphological evolution in mechanically processed ZnO + xC nanosystems as studied by EPR and photoluminescence spectroscopy *RSC Adv.* **6**

58709–22

[3] Willander M, Nur O, Zhao Q X, Yang L L, Lorenz M, Cao B Q, Zúñiga Pérez J, Czekalla C, Zimmermann G, Grundmann M, Bakin A, Behrends A, Al-Suleiman M, El-Shaer A, Che Mofor A, Postels B, Waag A, Boukos N, Travlos A, Kwack H S, Guinard J and Le Si Dang D 2009 Zinc oxide nanorod based photonic devices: recent progress in growth, light emitting diodes and lasers *Nanotechnology* **20** 332001

[4] Özgür U, Alivov Y I, Liu C, Teke a., Reshchikov M a., Doğan S, Avrutin V, Cho S-J and Morkoç H 2005 A comprehensive review of ZnO materials and devices *J. Appl. Phys.* **98** 41301

[5] Lee C J, Lee T J, Lyu S C, Zhang Y, Ruh H and Lee H J 2002 Field emission from well-aligned zinc oxide nanowires grown at low temperature *Appl. Phys. Lett.* **81** 3648–50

[6] Zimmler M A, Bao J, Capasso F, Müller S and Ronning C 2008 Laser action in nanowires: Observation of the transition from amplified spontaneous emission to laser oscillation *Appl. Phys. Lett.* **93** 51101

[7] Chou Y-H, Chou B-T, Chiang C-K, Lai Y-Y, Yang C-T, Li H, Lin T-R, Lin C-C, Kuo H-C, Wang S-C and Lu T-C 2015 Ultrastrong Mode Confinement in ZnO Surface Plasmon Nanolasers *ACS Nano* **9** 3978–83

[8] Sidiropoulos T P H, Röder R, Geburt S, Hess O, Maier S a., Ronning C and Oulton R F 2014 Ultrafast plasmonic nanowire lasers near the surface plasmon frequency *Nat. Phys.* **10** 870–6

[9] Nayeri F D, Soleimani E A and Salehi F 2013 Synthesis and characterization of ZnO

nanowires grown on different seed layers: The application for dye-sensitized solar cells *Renew. Energy* **60** 246–55

[10] Law M, Greene L E, Johnson J C, Saykally R and Yang P 2005 Nanowire dye-sensitized solar cells. *Nat. Mater.* **4** 455–9

[11] Opoku C, Hoettges K F, Hughes M P, Stolojan V, Silva S R P and Shkunov M 2013 Solution processable multi-channel ZnO nanowire field-effect transistors with organic gate dielectric *Nanotechnology* **24** 405203

[12] Govender K, Boyle D S, Kenway P B and O'Brien P 2004 Understanding the factors that govern the deposition and morphology of thin films of ZnO from aqueous solution *J. Mater. Chem.* **14** 2575

[13] Greene L E, Law M, Tan D H, Montano M, Goldberger J, Somorjai G and Yang P 2005 General Route to Vertical ZnO Nanowire Arrays Using Textured ZnO Seeds *Nano Lett.* **5** 1231–6

[14] Byrne D, McGlynn E, Kumar K, Biswas M, Henry M O and Hughes G 2010 A Study of Drop-Coated and Chemical Bath-Deposited Buffer Layers for Vapor Phase Deposition of Large Area, Aligned, Zinc Oxide Nanorod Arrays *Cryst. Growth Des.* **10** 2400–8

[15] Grabowska J, Nanda K K, McGlynn E, Mosnier J-P and Henry M O 2005 Studying the growth conditions, the alignment and structure of ZnO nanorods *Surf. Coatings Technol.* **200** 1093–6

[16] Park D J, Kim D C, Lee J Y and Cho H K 2006 Synthesis and microstructural characterization of growth direction controlled ZnO nanorods using a buffer layer

Nanotechnology **17** 5238–43

[17] Xu H, Wang H, Zhang Y, He W, Zhu M, Wang B and Yan H 2004 Hydrothermal synthesis of zinc oxide powders with controllable morphology *Ceram. Int.* **30** 93–7

[18] Ellmer K and Bikowski A 2016 Intrinsic and extrinsic doping of ZnO and ZnO alloys *J. Phys. D. Appl. Phys.* **49** 413002

[19] Davies G, Lightowlers E C, Woolley R, Newman R C and Oates a S 1984 Carbon in radiation damage centres in Czochralski silicon *J. Phys. C Solid State Phys.* **17** L499–503

[20] Thewalt M L W 2005 Spectroscopy of excitons and shallow impurities in isotopically enriched silicon—electronic properties beyond the virtual crystal approximation *Solid State Commun.* **133** 715–25

[21] Barba D, Koshel D, Martin F, Ross G G, Chicoine M, Schiettekatte F, Yedji M, Demarche J and Terwagne G 2010 Silicon nanocrystal synthesis by implantation of natural Si isotopes *J. Lumin.* **130** 669–73

[22] Manjón F J, Hernández-Fenollosa M a., Marí B, Li S F, Poweleit C D, Bell a., Menéndez J and Cardona M 2004 Effect of N isotopic mass on the photoluminescence and cathodoluminescence spectra of gallium nitride *Eur. Phys. J. B* **40** 453–8

[23] Zhang J M, Ruf T, Cardona M, Ambacher O, Stutzmann M, Wagner J-M and Bechstedt F 1997 Raman spectra of isotopic GaN *Phys. Rev. B* **56** 14399

[24] Meyer T ., Karaiskaj D, Thewalt M L . and Cardona M 2003 Effect of the isotopic mass of gallium on the indirect gap of GaP *Solid State Commun.* **126** 119–23

[25] Kreingol'd F I 1978 Dependence of the band gap of ZnO on the energy of zero point vibrations *Fiz. Tvend. Tela* **20** 3138–40

[26] Kreingol'd F I and Kulinkin B S 1986 Influence of isotopic substitution on the band gap of a ZnO crystal *Fiz. Tvend. Tela* **28** 3164

[27] Kreingol'd F I 1985 Influence of isotopic substitution of copper on the electron-phonon interaction on the Cu2O crystal *Fiz. Tvend. Tela* **27** 2839–41

[28] Kreingol'd F I, Lider K F and Shabaeva M B 1984 Influence of isotopic replacement of sulfur on the exciton spectrm of a CdS crystal *Fiz. Tvend. Tela (Leningrad)* vol 26(Cambridge)pp 3490–1

[29] Klochikhin A and Plekhanov V G 1980 Isotopic effects on Wannier-Mott exciton levels *Fiz. Tvend. Tela* **22** 585–8

[30] Plekhanov V G, Pustovarov V A, O'Connell-Bronin A A, Betenekova T A and Cholakh S O 1976 Excitions and characteristics of exciton-phonon interaction in LiH and LiD *Fiz. Tvend. Tela* **18** 2438–40

[31] Henderson B and Imbusch G F 1989 *Optical Spectroscopy of Inorganic Solids* ed H Frohlich, A J Heeger, P B Hirsch, N F Mott and R Brook (Oxford: Clarendon Press)

[32] Dingle R 1969 Luminescent Transitions Associated With Divalent Copper Impurities and the Green Emission from Semiconducting Zinc Oxide *Phys. Rev. Lett.* **23** 579–81

[33] Byrne D, Herklotz F, Henry M O and McGlynn E 2012 Unambiguous identification of the role of a single Cu atom in the ZnO structured green band *J. Physics. Condens. Matter* **24** 215802

[34] Heine V and Henry C 1975 Theory of the isotope shift for zero-phonon optical transitions at traps in semiconductors *Phys. Rev. B* **11** 3795

[35] Van Vechten J A 1976 Isotope shift at substitutional Cu in ZnO *Phys. Rev. B* **13** 946–9

[36] Dahan P, Fleurov V, Thurian P, Heitz R, Hoffmann A and Broser I 1998 Properties of the intermediately bound α - , β - and γ -excitons in ZnO:Cu *J. Phys. Condens. Matter* **10** 2007–19

[37] Morkoç H and Özgür U 2009 *Zinc Oxide Fundamentals, Materials and Device Technology* (Weinheim: Wiley-VCH)

[38] Gray C, Cullen J, Byrne C, Hughes G, Buyanova I, Chen W, Henry M O and McGlynn E 2015 Growth of isotopically enriched ZnO nanorods of excellent optical quality *J. Cryst. Growth* **429** 6–12

[39] Gray C, Trefflich L, Röder R, Ronning C, Henry M O and McGlynn E 2017 Growth of 18O isotopically enriched ZnO nanorods by two novel VPT methods *J. Cryst. Growth* **460** 85–93

[40] Biswas M, McGlynn E, Henry M O, McCann M and Rafferty a. 2009 Carbothermal reduction vapor phase transport growth of ZnO nanostructures: Effects of various carbon sources *J. Appl. Phys.* **105** 94306

[41] Peterson R B, Fields C L and Gregg B A 2004 Epitaxial Chemical Deposition of ZnO Nanocolumns from NaOH Solutions *Langmuir* **20** 5114–8

[42] Borchers C, Mu S, Stichtenoth D, Schwen D and Ronning C 2006 Catalyst - Nanostructure Interaction in the Growth of 1-D ZnO Nanostructures *J. Phys. Chem. B*

110 1656–60

[43] Hou D, Voss T, Ronning C, Menzel A and Zacharias M 2014 Deep-level emission in ZnO nanowires and bulk crystals: Excitation-intensity dependence versus crystalline quality *J. Appl. Phys.* **115** 233516

[44] Garces N Y, Wang L, Bai L, Giles N C, Halliburton L E and Cantwell G 2002 Role of copper in the green luminescence from ZnO crystals *Appl. Phys. Lett.* **81** 622

[45] Xing G, Xing G, Li M, Sie E J, Wang D, Sulistio A, Ye Q, Huan C H A, Wu T and Sum T C 2011 Charge transfer dynamics in Cu-doped ZnO nanowires *Appl. Phys. Lett.* **98** 102105

[46] Meyer B K, Alves H, Hofmann D M, Kriegseis W, Forster D, Bertram F, Christen J, Hoffmann A, Straßburg M, Dworzak M, Haboeck U and Rodina A V. 2004 Bound exciton and donor–acceptor pair recombinations in ZnO *Phys. Status Solidi* **241** 231–60

[47] Johnston K, Henry M O, McCabe D, McGlynn E, Dietrich M, Alves E and Xia M 2006 Identification of donor-related impurities in ZnO using photoluminescence and radiotracer techniques *Phys. Rev. B* **73** 165212

[48] Schilling M, Helbig R and Pensl G 1985 Bound exciton luminescence of Ar- and Al-implanted ZnO *J. Lumin.* **33** 201–12

[49] Cullen J, Byrne D, Johnston K, McGlynn E and Henry M O 2013 Chemical identification of luminescence due to Sn and Sb in ZnO *Appl. Phys. Lett.* **102** 192110

[50] Biswas M, Jung Y S, Kim H K, Kumar K, Hughes G J, Newcomb S, Henry M O and McGlynn E 2011 Microscopic origins of the surface exciton photoluminescence peak

in ZnO nanostructures *Phys. Rev. B* **83** 235320

[51] Müller S, Stichtenoth D, Uhrmacher M, Hofsäss H, Ronning C and Röder J 2007 Unambiguous identification of the PL-I[sub 9] line in zinc oxide *Appl. Phys. Lett.* **90** 12107

[52] Manjón F J, Mollar M, Hernández-Fenollosa M A, Marí B, Lauck R and Cardona M 2003 Effect of isotopic mass on the photoluminescence spectra of zinc oxide *Solid State Commun.* **128** 35–9

[53] Tsoi S, Lu X, Ramdas A K, Alawadhi H, Grimsditch M, Cardona M and Lauck R 2006 Isotopic-mass dependence of the A, B, and C excitonic band gaps in ZnO at low temperatures *Phys. Rev. B* **74** 165203

[54] Schubert E F, Göbel E O, Horikoshi Y, Ploog K and Queisser H J 1984 Alloy broadening in photoluminescence spectra of AlxGa1-xAs *Phys. Rev. B* **30** 813–20

[55] Solbrig C 1968 Dependence of emission spectrum of bound excitons in zinc oxide crystals on temperature and uniaxial stress *Z. Phys. A.* **211** 429–51